UNIVERSITÀ DI PARMA
ARCHIVIO DELLA RICERCA

University of Parma Research Repository

Timing Synchronization and Channel Estimation in Free-Space Optical OOK Communication Systems

This is the peer reviewd version of the followng article:

Original
Timing Synchronization and Channel Estimation in Free-Space Optical OOK Communication Systems / D'Amico, A. A.; Colavolpe, G.; Foggi, T.; Morelli, M.. - In: IEEE TRANSACTIONS ON COMMUNICATIONS. - ISSN 0090-6778. - 70:(2022), pp. 1901-1912. [10.1109/TCOMM.2022.3142134]

Availability:
This version is available at: 11381/2914953 since: 2022-03-18T08:32:08Z

Publisher:
Institute of Electrical and Electronics Engineers Inc.

Published
DOI:10.1109/TCOMM.2022.3142134

Terms of use:

Anyone can freely access the full text of works made available as "Open Access". Works made available

Publisher copyright

note finali coverpage

(Article begins on next page)

18 April 2024

Timing Synchronization and Channel Estimation in Free-Space Optical OOK Communication Systems

Antonio A. D'Amico, Giulio Colavolpe, Tommaso Foggi, Michele Morelli

Abstract

Fast and reliable synchronization in free-space optical (FSO) communications is a crucial task that has received little attention so far. Since in these applications the data rate is much higher than in traditional radio-frequency (RF) systems, novel technological contraints may arise in the design of the synchronization algorithms, as for example the need to operate at symbol rate instead with an oversampled data stream.

In this work, we consider an FSO link and investigate the problem of channel estimation, symbol timing recovery and frame detection using a known synch pattern. The modulation format is on-off keying (OOK) and the received signal is plagued by a mixture of thermal and shot noise. By applying the least-squares criterion, we derive a novel synchronization scheme that can jointly retrieve all the unknown parameters using symbol-spaced samples. Although designed without taking the noise statistics into account, the estimator performance is assessed in a realistic scenario where shot noise is present. Comparisons are made with the relevant Cramér-Rao bound for the joint estimation of the synchronization parameters and signal-dependent noise variances. This bound is not available in the literature and represents a further contribution of our work.

Numerical simulations and complexity analysis indicate that the resulting scheme performs satisfactorily with an affordable processing load. Hence, it represents a promising solution for fast synchronization in high-speed FSO communications.

Antonio A. D'Amico (antonio.damico@unipi.it) and Michele Morelli (michele.morelli@unipi.it) are with the Dipartimento di Ingegneria dell'Informazione of the University of Pisa. Giulio Colavolpe (giulio.colavolpe@unipr.it) and Tommaso Foggi (tommaso.foggi@unipr.it) are with the University of Parma, Department of Engineering and Architecture, viale delle Scienze 181/A, 43124 Parma, Italy, and CNIT Research Unit, I-43124 Parma, Italy.

I. Introduction

Free-space optical (FSO) communication is a promising technology to meet the increasing demand for data services. Compared to conventional radio-frequency (RF) transmissions, it offers the opportunity of license-free access, high security level, increased data rates and improved resilience to interference and jamming [1], [2]. Thanks to the aforementioned advantages, FSO has been suggested for both line-of-sight (LOS) wireless terrestrial links and satellite applications [3]. More recently, the use of this technology has been investigated for downlink transmissions from low-Earth-orbit (LEO) satellites to ground stations [4], [5].

One major challenge encountered in an FSO link is the susceptibility to atmospheric turbulence caused by a non-uniform distribution of the temperature and pressure along the transmission path. Such a phenomenon, known as scintillation, generates random fluctuations in the amplitude and phase of the received light, similar to the channel fading experienced in RF transmissions, with a coherence time ranging from 0.1 to 10 ms [6]. Furthermore, adverse wheather conditions like rain, fog and smoke, may result into a remarkable attenuation of the received optical power [7]. In these scenarios, interleaving and forward error correction coding become mandatory for reliable data reception. Since successful data decoding requires a proper design of the detection thresholds as well as the correct localization of the codewords within the received sample stream, accurate channel state information and timing synchronization is needed at the receiver. In digital communications, the timing synchronization process is typically split into two successive steps. The first one, called *bit synchronization*, looks for the optimum sampling instants where the output from the matched filter is maximum. The second one, called *frame synchronization*, is implemented by inserting a known training pattern, called unique word (UW), into the transmitted data sequence and searching for its position in the received waveform.

Most available schemes for bit synchronization in optical links are mainly conceived for continuous transmissions and employ a classical non-data-aided (NDA) or decision directed (DD) closed-loop (CL) structure. The timing error detector, which is the core device of any CL scheme, is typically designed through some heuristic approach or by resorting to classical techniques, including the early-late gate synchronizer [8], the Gardner algorithm [9] or the Mueller & Müller method [10]. Prominent examples in this category are found in [11] for pulse-position modulation (PPM), in [12]-[14] for on-off keying (OOK) signaling and in [15] for optical signals with a large dynamic range. As an alternative to CL methods, NDA open-loop (OL) algorithms have

been suggested in [16] in the context of 2-PPM modulation and in [17] for OOK signaling. Joint bit synchronization and data detection for PPM and OOK systems is proposed in [18] by resorting to the ML estimation principle. The resulting scheme is computationally demanding as it applies the Viterbi algorithm to a specified trellis diagram.

Once bit synchronization has been acquired, frame alignment is typically achieved by correlating the received symbol stream with a local copy of the UW. In [19], the authors derive the optimum maximum likelihood (ML) rule for frame detection by extending the pioneering work of Massey [20] to a Poisson optical channel. A high signal-to-noise ratio (SNR) approximation of the ML rule can be found in [21]. More recently, the issue of UW recognition has been investigated in [22] for an OOK system affected by shot noise, where the noise power is higher for a received 1 than for a received 0. The main drawback of this scheme is that it requires knowledge of the channel fading coefficient and signal dependent noise variances, which must be recovered in some manner. One possible solution is presented in [23], where the joint estimation of all the unknown parameters is embedded into the UW detection process.

In packet-based transmissions, data-aided (DA) OL algorithms are the favourite choice for fast clock recovery. On one hand, they exhibit improved accuracy with respect to NDA methods. On the other hand, they provide the timing estimate at the end of a specified observation window, while CL schemes are characterized by a prolonged acquisition period which is hardly consistent with this kind of applications. More importantly, DA-OL methods offer the opportunity to combine bit and frame synchronization into a single-step operation, which make them particularly attactive for applications where fast timing acquisition is required. In many packet radio systems, joint bit and frame synchronization is achieved by oversampling the received signal at a frequency multiple of the symbol rate and feeding the resulting stream to a sliding window correlator. The timing estimate is eventually obtained by searching for the maximum from the correlator. This approach was recently suggested in [24] for visible light communications and in [25] for bandlimited optical channels. In high-speed FSO communications, however, the oversampling operation may represent a critical issue, asking for expensive hardware equipments or some form of parallel implementation [26]. In these applications, it is highly desirable to achieve fast timing recovery through signal samples taken at symbol rate in order to relax the hardware constraints.

The presence of the preamble is also useful to acquire channel state information. Observing that in satellite systems long codewords with length of tens or hundreds of milliseconds are commonly used, the coherence time of the FSO channel can be in the order of a few data

blocks. Accordingly, a new channel estimate is needed at every new received codeword in order to optimally set the threshold levels for data decoding. Some methods for estimating the channel attenuation in an FSO link are illustrated in [23] and [25].

In this paper, we investigate the synchonization problem in a packet-based FSO communication link. We consider OOK signaling and assume that an avalanche photo-diode (APD) is employed as a photodetector at the receiver side. In particular, we look for some feasible architecture that exhibits the following two desirable properties: 1) bit synchronization, frame detection and channel estimation is achieved in a *joint* fashion so as to speed-up the timing acquisition process; 2) symbol rate samples are used to complete the synchronization task so as to reduce the sampling rate of the hardware as much as possible, which is especially desirable in high-speed communications. To the best of our knowledge, these features cannot be simultaneously found in any timing recovery scheme available in the literature. In order to meet such stringent requirements, we concentrate on the class of DA-OL schemes and assume that a UW is periodically embedded in the bitstream. Since the APD introduces shot noise with signal-dependent power, the system model is the same adopted in [22], except that no prior knowledge is assumed regarding the mean signal level and noise power. A first contribution of our work is the evaluation of the Cramér-Rao bound (CRB) for the joint estimation of the timing offset, channel attenuation and noise variances. This result is not available in the literature and proves to be useful for the analysis and design of synchronization schemes that are found to operate in the presence of shot noise. Although a bound for joint timing and channel recovery has previously been presented in [25], it only applies to signals plagued by thermal noise with signal independent power. The second contribution is the derivation of a new synchronization algorithm which determines the position of the UW and jointly provides estimates of the channel coefficient and timing offset in a closed form. The proposed method is based on the least squares (LS) estimation principle, which makes no assumption about the noise statistics. This approach has the advantage of leading to a practical scheme that provides *fast* synchronization with *symbol rate* sampling, as requested in high-speed communications. Compared to the optimum ML appoach, it results into some performance loss as it ignores any useful information conveyed by the signal-dependent noise power regarding the time instants at which a bit transition occurs. The loss is quantified by comparing the accuracy of the proposed method with the relevant CRB. It is worth noting that this is the first time that a timing recovery scheme is tested in the presence of signal-dependent noise power.

The rest of the paper is organized as follows. Next section introduces the system model and some basic notation. In Sect. III, we present the proposed synchronization algorithm and assess its processing requirement. The CRB analysis for the joint estimation of all unknown parameters, including the noise variances, is conducted in Sect. IV. We discuss simulation results in Sect. V and offer some conclusions in Sect. VI.

Notation: Matrices and vectors are denoted by boldface letters, $\mathbf{A}^{-1}$ is the inverse of a matrix $\mathbf{A}$ and $\|\mathbf{v}\|$ the norm of a vector $\mathbf{v}$. We use $\mathrm{E}\{\cdot\}$ to indicate the statistical expectation, while $(\cdot)^T$ is the transposition operator. The symbol $\otimes$ is adopted for the continuous-time convolution and, finally, we denote by $\tilde{\lambda}$ a trial value of an unknown parameter λ.

II. System Model

In this section, we first introduce the mathematical model of the photocurrent signal produced by the APD (continuous-time signal model). Next, we provide the analytical expression of the sample stream at the output of the receive filter (discrete-time signal model).

A. Continuous-time signal model

We consider a packet-based FSO communication link employing a non-return-to-zero (NRZ) OOK modulation format. The transmitted signal is expressed by

$$s(t) = \sum_i a_i p(t - iT) \tag{1}$$

where T is the signaling period, $a_i \in \{0, 1\}$ denotes the ith binary data symbol and $p(t)$ is a normalized rectangular shaping pulse with unit energy

$$p(t) = \begin{cases} 1/\sqrt{T} & 0 \le t \le T \\ 0 & \text{otherwise.} \end{cases} \tag{2}$$

Data transmission is organized in successive frames, each of which consists of N_F symbol periods. In order to mark the start of each frame, a UW of L pilot symbols is periodically inserted in the transmitted data stream. Without loss of generality, we assume that the pilots in (1) have indices $i \in \{0, 1, \ldots, L-1\}$ and are collected into a vector $\mathbf{a}_{UW} = [a_0, a_1, \ldots, a_{L-1}]$.

At the receiver side, an APD is used for direct detection of the transmitted data. The photocurrent signal provided by the APD is proportional to the intensity of the incoming field and is given by

$$r(t) = hs(t - \tau) + w_0(t) + w_{sh}(t) \tag{3}$$

where h is the channel state, τ is an unknown delay specifying the UW position in the receiver time scale, $w_0(t)$ accounts for thermal noise and, finally, $w_{sh}(t)$ represents the shot noise introduced by the APD, which is statistically independent of $w_0(t)$. The channel coefficient h is related to the average received optical power P_{avg} by the following relationship

$$h = \frac{2RP_{\text{avg}}\sqrt{T}}{e} \tag{4}$$

where R denotes the APD responsivity and $e = 1.60217662 \cdot 10^{-19}$ is the electron charge (in coulombs). Due to the atmospheric turbulence encountered in both terrestrial and satellite FSO links, the received optical power suffers from random fluctuations which may result into significant signal fading. Accordingly, the receiver has no prior knowledge of the channel realization h, which must therefore be regarded as an unknown parameter. In practical applications, the coherence time of the channel fluctuations varies from 0.1 to 10 ms, while the signalling rate can be as large as hundreds or thousands of Mbps [3]. In such a case, we can confidently assume that h remains constant over many symbol periods and, in particular, over a frame interval.

The thermal noise $w_0(t)$ is modeled as a white Gaussian process with one-sided power spectral density N_0 expressed by

$$N_0 = \frac{i_{\text{th}}^2}{e^2 M^2} \tag{5}$$

where i_{th} denotes the current thermal density and M is the APD multiplication factor. While thermal noise is present in $r(t)$ at any time instant, shot noise only appears when a unitary symbol $a_i = 1$ is received. Hence, we can express $w_{sh}(t)$ in (3) as

$$w_{sh}(t) = \sqrt{T}\eta_{sh}(t)\sum_i a_i p(t - \tau - iT) \tag{6}$$

where $\eta_{sh}(t)$ is a white Gaussian process with one-sided power spectral density N_{sh}. The latter depends on the channel fading coefficient through

$$N_{sh} = \frac{2Fh}{\sqrt{T}} \tag{7}$$

with F denoting the APD noise figure. Finally, denoting by $w(t) = w_0(t) + w_{sh}(t)$ the overall noise contribution, from (3) and (6) we have

$$w(t) = \sqrt{T}\left[w_0(t)\sum_i (1 - a_i)p(t - \tau - iT) + w_1(t)\sum_i a_i p(t - \tau - iT)\right] \tag{8}$$

where $w_1(t) = w_0(t) + \eta_{sh}(t)$ has power spectral density $N_1/2$, with $N_1 = N_0 + N_{sh}$, and we have used the identity

$$\sqrt{T}\sum_i p(t - \tau - iT) \equiv 1. \tag{9}$$

B. Discrete-time signal model

In a typical OOK receiver for FSO communications, the photocurrent signal $r(t)$ is integrated over each bit period before further processing. This is achieved by passing $r(t)$ through an integrate-and-dump filter (IDF), where the dumping operation is performed once per symbol interval. Although symbol rate operation is a highly desirable feature in high-speed communications, it is important to assess its impact on the performance of synchronization algorithms. For this reason, in the subsequent analysis we consider a more flexible setting in which the integrator output is dumped with period $T_c = T/N$, where $N \geq 1$ is the oversampling factor. By selecting different values of N, we can disclose how much information is possibly lost when the symbol-spaced samples are employed as observation variables.

The mathematical model of the signal provided by the IDF is obtained through the following procedure. Firstly, we call $x(t) = r(t) \otimes g(t)$ the waveform obtained by feeding $r(t)$ to a rectangular filter with impulse response

$$g(t) = \begin{cases} 1/\sqrt{T} & 0 \leq t \leq T_c \\ 0 & \text{otherwise} \end{cases} \tag{10}$$

and denote by $x(k)$ the sample of $x(t)$ taken at $t_k = (k+1)T_c$. Secondly, we observe that the sequence $\{x(k)\}$ is just the sample stream provided by the IDF. A simple expression for $x(k)$ can be found by rewriting $s(t)$ in (1) and $w(t)$ in (8) as

$$s(t) = \sum_i c_i g(t - iT_c) \tag{11}$$

and

$$w(t) = \sqrt{T}\left[w_0(t)\sum_i (1-c_i)g(t-\tau-iT_c) + w_1(t)\sum_i c_i g(t-\tau-iT_c)\right] \tag{12}$$

where the quantities $\{c_i\}$ are obtained through the N-time repetition of each data symbol, i.e.,

$$c_i = a_{i\backslash N} \tag{13}$$

with $i\backslash N$ denoting the integer division of i by N. Using (13), the UW sequence $\mathbf{a}_{UW}$ is thus transformed into an $NL-$dimensional vector $\mathbf{c}_{UW} = [c_0, c_1, \ldots, c_{NL-1}]$. To proceed further, we decompose the delay τ as

$$\tau = k_0 T_c + \varepsilon T_c \tag{14}$$

where k_0 is a non-negative integer called *integer timing offset*, while $\varepsilon \in [0, 1)$ is the *fractional timing offset*. Then, sample $x(k)$ is expressed by

$$x(k) = \frac{1}{\sqrt{T}} \int_{kT_c}^{(k+1)T_c} [hs(\alpha - k_0 T_c - \varepsilon T_c) + w(\alpha)] d\alpha \tag{15}$$

which, after standard computations and bearing in mind (11) and (12), can be rewritten as

$$x(k) = \frac{h}{N} d_{k-k_0}(\varepsilon) + n(k). \tag{16}$$

In the above expression, we have defined

$$d_k(\varepsilon) = c_k + \varepsilon b_k \tag{17}$$

with

$$b_k = c_{k-1} - c_k \tag{18}$$

while the noise terms $\{n(k)\}$ are statistically independent random variables. When conditioned to $d_{k-k_0}(\varepsilon)$, they are Gaussian distributed with zero-mean and variance

$$\sigma_n^2(k - k_0, \varepsilon, N_0, N_1) = \frac{N_0}{2N}[1 - d_{k-k_0}(\varepsilon)] + \frac{N_1}{2N} d_{k-k_0}(\varepsilon). \tag{19}$$

III. Estimation of the synchronization parameters

A. Problem formulation

In order to establish the communication link, the receiver must preliminarily activate a synchronization procedure so as to correctly align its time scale to the incoming signal. This is achieved by recovering the timing offsets k_0 and ε, which provide frame and bit synchronization, respectively. Channel state information is also necessary for the design of the optimum thresholds employed in the data detection process. In this section, we show how to complete such a synchronization task. As mentioned previously, we look for a solution that can operate even in the absence of any oversampling ($N = 1$) and is able to estimate the unknown parameters $\{k_0, \varepsilon, h\}$ in a joint fashion in order to achieve fast timing acquisition. For this purpose, we divide the sequence $\{x(k)\}$ into overlapped segments of length NL equal to the dimension of vector $\mathbf{c}_{UW}$. Each segment corresponds to a different hypothesized value $\tilde{k}_0$ of the integer timing offset and is denoted by $\mathbf{x}(\tilde{k}_0) = [x(\tilde{k}_0), x(\tilde{k}_0 + 1), \ldots, x(\tilde{k}_0 + NL - 1)]^T$. The length NL is chosen such that, when $\tilde{k}_0 = k_0$, the observation vector $\mathbf{x}(k_0)$ contains the whole UW, while minimizing the contamination from unknown information-bearing symbols. Assuming that the

UW is present in each frame of length $T_F = N_F T$, the search for the UW position can be restricted to the interval $\tilde{k}_0 \in I$, with $I = \{0, 1, 2, \ldots, N_F N - 1\}$.

Intuitively speaking, the presence of shot noise may prove useful for the purpose of timing recovery due to the abrupt variation of the noise power induced by a transition $1 \to 0$ or $0 \to 1$ in the entries of $\mathbf{c}_{UW}$. The ML estimation principle provides the optimal way for exploiting information conveyed by such noise power fluctuations. Unfortunately, the exact ML solution for the problem at hand leads to a computationally intractable multi-dimensional optimization process, thereby motivating the search for some alternative suboptimal methods. For this reason, in what follows the synchronization parameters are recovered by resorting to the LS concept, which makes no assumption on the noise statistics. The impact of shot noise on the performance of the resulting schemes will be assessed later by means of computer simulations.

From (16), the entries of $\mathbf{x}(k_0)$ are given by

$$x(k + k_0) = h(\alpha_k + \varepsilon\beta_k) + n(k + k_0) \qquad 0 \le k \le NL - 1 \tag{20}$$

with

$$\alpha_k = \frac{1}{N} c_k \tag{21}$$

and

$$\beta_k = \frac{1}{N}(c_{k-1} - c_k) = \alpha_{k-1} - \alpha_k. \tag{22}$$

Letting $\boldsymbol{\alpha} = [\alpha_0, \alpha_1, \ldots, \alpha_{NL-1}]^T$ and $\boldsymbol{\beta} = [\beta_0, \beta_1, \ldots, \beta_{NL-1}]^T$, we can put (20) in matrix form as

$$\mathbf{x}(k_0) = h(\boldsymbol{\alpha} + \varepsilon\boldsymbol{\beta}) + \mathbf{n}(k_0) \tag{23}$$

where $\mathbf{n}(k_0) = [n(k_0), n(k_0 + 1), \ldots, n(k_0 + NL - 1)]^T$ is the noise vector. It is worth noting that vector $\boldsymbol{\alpha}$ is totally specified by the UW elements collected into $\mathbf{a}_{UW}$, while $\boldsymbol{\beta}$ depends on the sequence $\{a_{-1}, a_0, \ldots, a_{L-1}\}$, which is known except possibly for a_{-1}. To simplify the discussion we set $a_{-1} = 0$, which amounts to assuming that a null pilot symbol is inserted in front of the UW. This way, the entries of $\boldsymbol{\alpha}$ and $\boldsymbol{\beta}$ can be considered as known quantities at the receiver.

The LS estimation procedure is now applied to vectors $\mathbf{x}(\tilde{k}_0)$ (with $\tilde{k}_0 \in I_{k_0}$) for jointly retrieving the synchronization parameters $\{k_0, \varepsilon, h\}$.

B. Least-squares estimation

From the mathematical model of $\mathbf{x}(k_0)$ given in (23), the LS estimate of $\{k_0, \varepsilon, h\}$ is obtained by looking for the global minimum of the objective function

$$\Phi_{LS}(\tilde{k}_0, \tilde{\varepsilon}, \tilde{h}) = \left\| \mathbf{x}(\tilde{k}_0) - \tilde{h}(\boldsymbol{\alpha} + \tilde{\varepsilon}\boldsymbol{\beta}) \right\|^2. \tag{24}$$

The minimum is found through the following procedure. We begin by keeping $\tilde{k}_0$ fixed and let $\tilde{\varepsilon}$ and $\tilde{h}$ vary. Hence, putting to zero the derivatives of $\Phi_{LS}(\tilde{k}_0, \tilde{\varepsilon}, \tilde{h})$ with respect to $\tilde{\varepsilon}$ and $\tilde{h}$ yields

$$\hat{\varepsilon}(\tilde{k}_0) = \frac{Av(\tilde{k}_0) - Cu(\tilde{k}_0)}{Bu(\tilde{k}_0) - Cv(\tilde{k}_0)} \tag{25}$$

$$\hat{h}(\tilde{k}_0) = \frac{Bu(\tilde{k}_0) - Cv(\tilde{k}_0)}{AB - C^2} \tag{26}$$

where $u(\tilde{k}_0)$ and $v(\tilde{k}_0)$ are obtained from the observation vector $\mathbf{x}(\tilde{k}_0)$ as

$$u(\tilde{k}_0) = \boldsymbol{\alpha}^T \mathbf{x}(\tilde{k}_0) \tag{27}$$

$$v(\tilde{k}_0) = \boldsymbol{\beta}^T \mathbf{x}(\tilde{k}_0) \tag{28}$$

while the coefficients

$$A = \|\boldsymbol{\alpha}\|^2 \tag{29}$$

$$B = \|\boldsymbol{\beta}\|^2 \tag{30}$$

$$C = \boldsymbol{\alpha}^T \boldsymbol{\beta} \tag{31}$$

can be precomputed and stored in the receiver. We proceed further by plugging the results (25) and (26) back into (24). This yields the LS metric for the estimation of k_0 in the form

$$\Psi_{LS}(\tilde{k}_0) = \left\| \mathbf{x}(\tilde{k}_0) \right\|^2 - \frac{Av^2(\tilde{k}_0) + Bu^2(\tilde{k}_0) - 2Cu(\tilde{k}_0)v(\tilde{k}_0)}{AB - C^2}. \tag{32}$$

As a final step, we suggest to normalize $\Psi_{LS}(\tilde{k}_0)$ to the energy $\left\| \mathbf{x}(\tilde{k}_0) \right\|^2$ of the sliding observation window. Such an operation has a couple of advantages. On one hand, it allows one to control the dynamic range of the metric, which otherwise increases with NL. On the other hand, extensive simulations indicate that the normalization process leads to improved system performance. The estimate of k_0 is eventually obtained as

$$\hat{k}_0 = \arg \max_{\tilde{k}_0 \in I_{k_0}} \left\{ \Gamma_{LS}(\tilde{k}_0) \right\}. \tag{33}$$

with

$$\Gamma_{LS}(\tilde{k}_0) = \frac{Av^2(\tilde{k}_0) + Bu^2(\tilde{k}_0) - 2Cu(\tilde{k}_0)v(\tilde{k}_0)}{(AB - C^2)\left\|\mathbf{x}(\tilde{k}_0)\right\|^2}. \tag{34}$$

Once $\hat{k}_0$ is available, it is used in (25) and (26) to get the estimates of ε and h. We refer to the above procedure as the least-squares estimator (LSE) of the timing offset and signal amplitude.

C. Remarks

1) Although derived for a general oversampling factor N, LSE can provide joint bit and frame synchronization from symbol-spaced samples ($N = 1$). This makes it particularly attractive for fast timing recovery in high-speed FSO communications. After a careful review of the related literature, we were not able to find any other scheme exhibiting such favourable advantages.

2) The aforementioned features of LSE are a consequence of the signal model shown in (23). This means that this scheme is suitable for OOK transmissions, while it cannot be applied in the presence of bandlimited pulse shaping and/or multilevel signaling formats.

3) An alternative approach for timing acquisition is to split the bit and frame synchronization tasks into two successive stages. In particular, bit synchronization can be firstly accomplished by resorting to any conventional NDA-OL scheme, as for example the celebrated Oerder and Meyr estimator (OME) reported in [27]. This provides a timing estimate which is subsequently used to adjust the phase of the sampling device. Frame acquisition is eventually acquired by correlating the symbol rate samples with a local copy of the UW. Compared to LSE, this approach results into a prolonged acquisition as a consequence of its two-stage structure. Furthermore, all the available NDA-OL timing estimators require a large enough oversampling factor, which may be a serious concern in FSO applications.

4) The joint estimation of the timing and channel parameters $\{k_0, \varepsilon, h\}$ was previously investigated in [25] for bandlimited optical intensity channels. The resulting scheme, denoted as the Gappmair estimator (GE), is based on the ML estimation principle and can easily be adapted to OOK transmissions as well. It basically employs a grid-search to locate the maximum of the correlation between the UW and the received sample stream. A parabolic interpolation is eventually used for a fine identification of the correlation peak A major drawback of this method is that a sufficiently large oversampling factor must be selected to avoid aliasing problems.

TABLE I

COMPUTATIONAL REQUIREMENTS OF THE DIFFERENT ESTIMATORS

Estimators	Number of flops per symbol period
LSE	$N(NL_0 + L_T + 11)$
GE	$N(NL_0 - 1)$
OME	$L_0 + 4N - 1$

D. Complexity analysis

In assessing the processing requirement of LSE, we observe that the entries of $\boldsymbol{\alpha}$ and $\boldsymbol{\beta}$ belong to the set $\{-1/N, 0, 1/N\}$, so that no multiplication is needed to compute $u(\tilde{k}_0)$ and $v(\tilde{k}_0)$ from (27) and (28). In particular, denoting by L_0 the number of unitary symbols in $\mathbf{a}_{UW}$, it turns out that $u(\tilde{k}_0)$ is obtained with $NL_0 - 1$ additions, while $v(\tilde{k}_0)$ is evaluated through $L_T - 1$ additions, where L_T is the overall number of transitions $1 \to 0$ and $0 \to 1$ in the entries of $\mathbf{a}_{UW}$. As for the signal energy $\left\|\mathbf{x}(\tilde{k}_0)\right\|^2$, it can be recursively updated by means of the following iterative equation

$$\left\|\mathbf{x}(\tilde{k}_0)\right\|^2 = \left\|\mathbf{x}(\tilde{k}_0 - 1)\right\|^2 + x^2(\tilde{k}_0 + NL - 1) - x^2(\tilde{k}_0 - 1) \tag{35}$$

with only two multiplications and two additions. Assuming that the coefficients A, B, C are available, the metric $\Gamma_{LS}(\tilde{k}_0)$ is next obtained with 7 supplementary products and 2 additions. The computation of $\hat{\varepsilon}(\hat{k}_0)$ and $\hat{h}(\hat{k}_0)$ is not accounted for since these quantities are only evaluated once at the end of the estimation procedure. Summarizing all the above results, it turns out that the overall complexity of LSE amounts to $N(NL_0 + L_T + 2)$ additions plus $9N$ multiplications for each symbol period.

The timing metric employed by GE is the oversampled correlation between the APD photocurrent signal and a local copy of the UW, which is accomplished through $N(NL_0 - 1)$ additions every symbol period. As for OME, it requires 2 real multiplications plus 2 real additions for each received sample. Hence, performing timing synchronization through OME followed by the symbol rate correlation with the UW requires $2N$ multiplications and $L_0 + 2N - 1$ additions for each symbol interval. The complexity of the investigated schemes is summarized in Tab. I in terms of floating point operations (flops).

IV. CRB ANALYSIS

It is interesting to compare the performance of LSE with the relevant CRB. While the derivation of LSE has been previously conducted without taking the presence of shot noise into account, we now consider a more realistic scenario where the noise power is modeled as reported in (19). Inspection of (7) reveals that the power spectral density of the shot noise is strictly related to the channel fading coefficient h and the APD noise figure F. Although such a relationship can reduce the number of unknown parameters involved in the estimation procedure, it is not considered in the subsequent analysis. The reason is that in practice only the nominal value of F is known, while its exact value is not available due to long-term fluctuations arising from possible modifications of the operating conditions. Random fluctuations are also expected in the terms i_{th} and M appearing in (5), which make N_0 an unknown quantity. Putting these facts together, we conclude that the terms $\{h, N_0, N_1\}$ can reasonably be treated as independent unknown parameters. Accordingly, in this section we evaluate the CRB for the joint estimation of $\{\varepsilon, h, N_0, N_1\}$. Such a bound is not available in the literature and represents a major outcome of our study. In the foregoing analysis, we assume that the integer-valued parameter k_0 has been successfully detected and, without any loss of generality, is fixed to zero. Furthermore, we let $\mathbf{x}(k_0) = \mathbf{x}$ to simplify the notation.

Putting $k_0 = 0$ into (16) and (19), yields

$$x(k) = \frac{h}{N} d_k(\varepsilon) + n(k) \tag{36}$$

where the noise terms $\{n(k)\}$ are Gaussian distributed with zero-mean and variance

$$\sigma_n^2(k, \varepsilon, N_0, N_1) = \frac{N_0}{2N}[1 - d_k(\varepsilon)] + \frac{N_1}{2N} d_k(\varepsilon). \tag{37}$$

Hence, the log-likelihood function (LLF) of $\mathbf{x}$ is given by

$$\Lambda(\varepsilon, h, N_0, N_1) = -\frac{1}{2} \sum_{k=0}^{NL-1} \left\{ \ln[\sigma_n^2(k, \varepsilon, N_0, N_1)] + \frac{[x_k - h d_k(\varepsilon)/N]^2}{\sigma_n^2(k, \varepsilon, N_0, N_1)} \right\}. \tag{38}$$

The Fisher information matrix (FIM) stemming from $\Lambda(\varepsilon, h, N_0, N_1)$ is computed in Appendix A. Unfortunately, its expression is rather cumbersome and cannot be inverted in a closed-form. The analysis becomes much easier when $\varepsilon = 0$. To see how this comes about, we observe that such a specific situation leads to $d_k = c_k$ and

$$\sigma_n^2(k, \varepsilon, N_0, N_1) = \frac{N_0}{2N}(1 - c_k) + \frac{N_1}{2N} c_k. \tag{39}$$

Furthermore, we define the two sets $\mathcal{U}_0 = \{k \in \{0, 1, \ldots, NL-1\} : c_k = 0\}$ and $\mathcal{U}_1 = \{k \in \{0, 1, \ldots, NL-1\} : c_k = 1\}$, collecting the indices k for which the pilot symbol c_k is either 0 or 1. Let NL_1 and NL_0 be the cardinality of $\mathcal{U}_1$ and $\mathcal{U}_0$, respectively, where L_0 and L_1 denote the number of unitary and null symbols in $\mathbf{a}_{UW}$. Then, we can rewrite (72)-(75) as

$$[\mathbf{F}_{\boldsymbol{\varphi}}]_{1,1} = \frac{(N_1 - N_0)^2}{2}\left(\frac{K_0}{N_0^2} + \frac{K_1}{N_1^2}\right) + \frac{2h^2}{N}\left(\frac{K_0}{N_0} + \frac{K_1}{N_1}\right) \tag{40}$$

$$[\mathbf{F}_{\boldsymbol{\varphi}}]_{2,2} = \frac{2L_1}{N_1} \tag{41}$$

$$[\mathbf{F}_{\boldsymbol{\varphi}}]_{3,3} = \frac{NL_0}{2N_0^2} \tag{42}$$

$$[\mathbf{F}_{\boldsymbol{\varphi}}]_{4,4} = \frac{NL_1}{2N_1^2} \tag{43}$$

where

$$K_0 = \sum_{k \in \mathcal{U}_0} c_{k-1}^2 = \sum_{k \in \mathcal{U}_0} c_{k-1} \tag{44}$$

and

$$K_1 = \sum_{k \in \mathcal{U}_1} (c_{k-1} - 1)^2 = \sum_{k \in \mathcal{U}_1} (1 - c_{k-1}) = NL_1 - \sum_{k \in \mathcal{U}_1} c_{k-1}. \tag{45}$$

Collecting (44) and (45), yields

$$K_0 - K_1 = \sum_{k=0}^{NL-1} c_{k-1} - NL_1 = c_{-1} - c_{NL-1} \tag{46}$$

which reduces to $K_0 = K_1$ when $c_{-1} = c_{NL-1}$. We also observe that K_0 represents the number of transitions $1 \to 0$ in the UW sequence and its maximum value is thus $L/2$. In the following derivations, we put $K_0 = K_1 = \rho L/2$, with $\rho \leq 1$. Hence, we can rewrite (40) as $[\mathbf{F}_{\boldsymbol{\varphi}}]_{1,1} = \rho\mu_\varepsilon$, with

$$\mu_\varepsilon = \frac{L}{4}\left[\frac{(N_1 - N_0)^2(N_0^2 + N_1^2)}{N_0^2 N_1^2} + \frac{4h^2(N_0 + N_1)}{NN_0N_1}\right] \tag{47}$$

while the other entries of the FIM shown in (76)-(80) become

$$[\mathbf{F}_{\boldsymbol{\varphi}}]_{1,2} = -\frac{\rho hL}{NN_1} \tag{48}$$

$$[\mathbf{F}_{\boldsymbol{\varphi}}]_{1,3} = \frac{\rho L(N_1 - N_0)}{4N_0^2} \tag{49}$$

$$[\mathbf{F}_{\boldsymbol{\varphi}}]_{1,4} = -\frac{\rho L(N_1 - N_0)}{4N_1^2} \tag{50}$$

$$[\mathbf{F}_{\boldsymbol{\varphi}}]_{2,3} = [\mathbf{F}_{\boldsymbol{\varphi}}]_{2,4} = [\mathbf{F}_{\boldsymbol{\varphi}}]_{3,4} = 0. \tag{51}$$

Summarizing all the above results, we note that the FIM takes the form

$$\mathbf{F}_{\boldsymbol{\varphi}} = \begin{bmatrix} \rho\mu_{\varepsilon} & \rho\mathbf{u}^T \\ \rho\mathbf{u} & \mathbf{A} \end{bmatrix} \tag{52}$$

where $\mathbf{A}$ is a diagonal matrix

$$\mathbf{A} = \text{diag}\left\{ \frac{2L_1}{N_1}, \frac{NL_0}{2N_0^2}, \frac{NL_1}{2N_1^2} \right\} \tag{53}$$

and $\mathbf{u}$ is a tridimensional vector

$$\mathbf{u} = \left[-\frac{hL}{NN_1} \ , \ \frac{L(N_1 - N_0)}{4N_0^2} \ , \ -\frac{L(N_1 - N_0)}{4N_1^2} \right]^T. \tag{54}$$

From (52), the inverse of $\mathbf{F}_{\boldsymbol{\varphi}}$ is found to be

$$\mathbf{F}_{\boldsymbol{\varphi}}^{-1} = \begin{bmatrix} \text{CRB}(\varepsilon) & -\text{CRB}(\varepsilon) \cdot \mathbf{v}^T \\ -\text{CRB}(\varepsilon) \cdot \mathbf{v} & \mathbf{B} \end{bmatrix} \tag{55}$$

where the bound for the estimation of ε is

$$\text{CRB}(\varepsilon) = \frac{1}{\rho\mu_{\varepsilon} - \rho^2(\mathbf{u}^T\mathbf{A}^{-1}\mathbf{u})} \tag{56}$$

with

$$\mathbf{u}^T\mathbf{A}^{-1}\mathbf{u} = \frac{L^2}{8N}\left[\frac{4h^2}{NN_1L_1} + (N_1 - N_0)^2 \left(\frac{1}{L_0N_0^2} + \frac{1}{L_1N_1^2} \right) \right]. \tag{57}$$

Furthermore, we have $\mathbf{v} = \rho \cdot (\mathbf{A}^{-1}\mathbf{u})$ and

$$\mathbf{B} = \left(\mathbf{A} - \frac{\rho}{\mu_{\varepsilon}} \cdot \mathbf{u}\mathbf{u}^T \right)^{-1} = \mathbf{A}^{-1} + [\text{CRB}(\varepsilon)]\mathbf{v}\mathbf{v}^T. \tag{58}$$

The diagonal elements of $\mathbf{B}$ provide the bounds for the estimation of (h, N_0, N_1) in the form

$$\text{CRB}(h) = \frac{N_1}{2L_1} + \left(\frac{\rho Lh}{2NL_1} \right)^2 \text{CRB}(\varepsilon) \tag{59}$$

$$\text{CRB}(N_0) = \frac{2N_0^2}{NL_0} + \left[\frac{\rho L(N_1 - N_0)}{2NL_0} \right]^2 \text{CRB}(\varepsilon) \tag{60}$$

$$\text{CRB}(N_1) = \frac{2N_1^2}{NL_1} + \left[\frac{\rho L(N_1 - N_0)}{2NL_1} \right]^2 \text{CRB}(\varepsilon) \tag{61}$$

which generalize the corresponding results obtained in [23] in the presence of ideal bit synchronization.

TABLE II

APD PARAMETERS

Parameter	Value
$i_{\rm th}$	10^{-12} [A/$\sqrt{\rm Hz}$]
F	5
R	0.9 [A/W]
M	20

V. SIMULATION RESULTS

A. Simulation set-up

Computer simulations have been run to assess the performance of the proposed synchronization scheme in a typical FSO scenario with a signalling rate of 10 Gbps. Direct detection of OOK symbols is achieved through an APD characterized by the parameters listed in Tab. II. The photocurrent signal is affected by both thermal and shot noise, with one-sided power spectral densities N_0 and N_{sh} as specified in (5) and (7), respectively. In particular, we observe that N_0 only depends on $i_{\rm th}$ and M, which are kept fixed throughout simulations. On the other hand, combining (4) and (7) yields

$$N_{sh} = \frac{4FR}{e} P_{\rm avg} \tag{62}$$

where $P_{\rm avg}$ is varied in the subsequent analysis so as to assess its impact on the system performance. Each data frame is composed by a payload section of $9L = 1143$ OOK symbols preceded by the UW. The latter is a maximum-length sequence with $L_1 = 64$ and $L_0 = 63$.

B. Performance assessment

A *failure* event is declared to occur whenever the timing estimation error is greater than $T/2$ in magnitude, which corresponds to an incorrect detection of the UW position within the observation window. The *failure probability* is thus defined as

$$P_f = \Pr\left\{|\hat{\tau} - \tau| > T/2\right\} \tag{63}$$

where τ is given in (14) and

$$\hat{\tau} = (\hat{k}_0 + \hat{\varepsilon}) T_c. \tag{64}$$

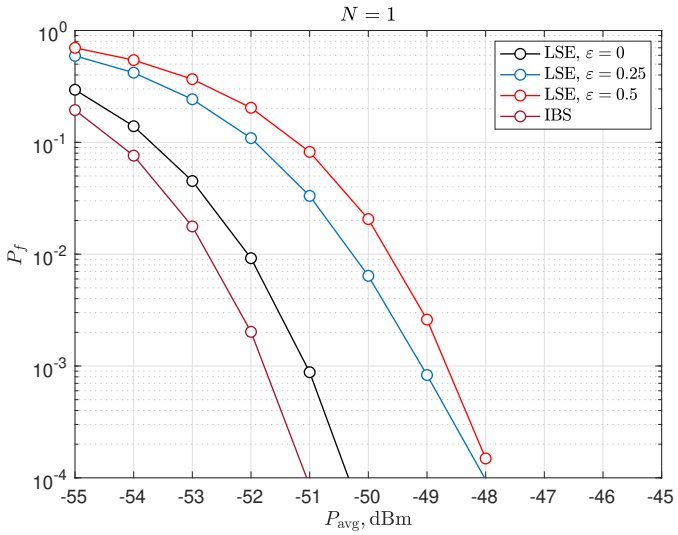

Fig. 1. Probability of failure as a function of P_{avg} for $N = 1$ and $\varepsilon = 0$, 0.25 and 0.5.

Fig. 1 illustrates P_f as a function of P_{avg}, expressed in decibel milliwatts (dBm), for $N = 1$ and $\varepsilon = 0$, 0.25 and 0.5. The curve labeled IBS (Ideal Bit Synchronization) is obtained under genie-aided FFO estimation (i.e., $\hat{\varepsilon} = \varepsilon = 0$) and looking for the maximum of the objective function (24) with respect to $(\tilde{k}_0, \tilde{h})$ after a normalization by $\left\|\mathbf{x}(\tilde{k}_0)\right\|^2$. As is seen, LSE achieves the best performance with $\varepsilon = 0$. In such a case, the loss with respect to the IBS curve is less than 1 dB, but increases to 3 dB when $\varepsilon = 0.5$. Intuitively speaking, the dependence of P_f on ε could be ascribed to the significant amount of intersymbol interference (ISI) that affects the entries of $\mathbf{x}(k_0)$ as ε approaches ± 0.5.

Although the main advantage of LSE is the possibility of operating with symbol-spaced samples, it is interesting to assess the impact of the oversampling factor N on the system performance. In Fig. 2 we show P_f versus P_{avg} when ε is uniformly distributed over $[0, 1)$ and $N = 1$, 2 and 4. These results indicate that a gain of nearly 1 dB is obtained in passing from $N = 1$ to $N = 2$, while no significant improvement can be attained by further increasing the oversampling factor. Observing that the use of symbol-spaced samples as observation variables results into a tolerable loss of the LSE performance, a good trade-off between system complexity and detection capability is achieved by choosing $N = 1$.

In Fig. 3 we compare LSE, GE and OME in terms of P_f vs. P_{avg}. The FFO is still uniformly distributed over $[0, 1)$ and each estimator operates with a specific value of N. In particular, the

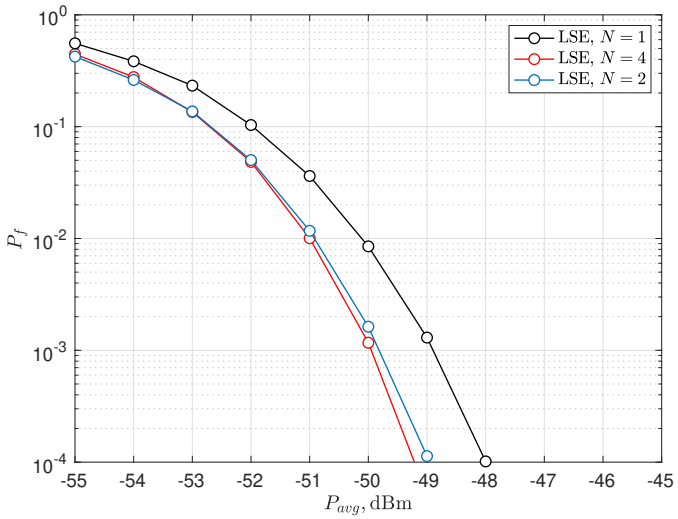

Fig. 2. Probability of failure as a function of ε, for three different values of P_{avg} and $N = 1$ or 2.

LSE curve is obtained with $N = 1$, while $N = 2$ is chosen for GE because this scheme cannot work in the absence of any signal oversampling. As for OME, it first retrieves bit synchronization by applying the algorithm in [27] to an observation window of length LT. In this stage $N = 4$ is used, which is the minimum oversampling factor leading to satisfactory performance. Frame detection is next accomplished using symbol-spaced samples taken at the adjusted time instants. We see that LSE outperforms the other schemes, while dispensing from any oversampling operation. At P_f values in the order of 10^{-3}, the gain with respect to OME is nearly 1.5 dB and increases to 3 dB when considering GE.

The accuracy of the channel estimates provided by LSE is measured in terms of their normalized mean square estimation error (NMSEE), which is defined as

$$\text{NMSEE}(h) = \text{E}\left\{\left(\frac{\hat{h} - h}{h}\right)^2\right\}. \tag{65}$$

In Fig. 4 we report NMSEE(h) for LSE, GE and OME as a function of P_{avg}. For each considered scheme, the oversampling factor is the same as in Fig. 3 and ε is still uniformly distributed over the range $[0, 1)$. The relevant CRB, computed from numerical inversion of the FIM, is also shown as a benchmark. It is worth pointing out that these results have been obtained by assuming ideal detection of the UW position, i.e., letting $\hat{k}_0 = k_0$. The reason is that measuring the channel estimation accuracy in the presence of a failure event is totally useless, as in such

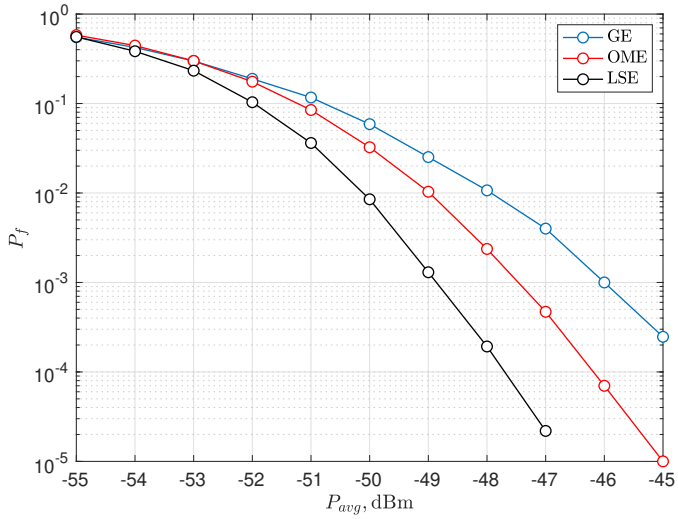

Fig. 3. Probability of failure for LSE, GE and OME as a function of P_{avg}, with ε uniformly distributed in $[0, 1)$.

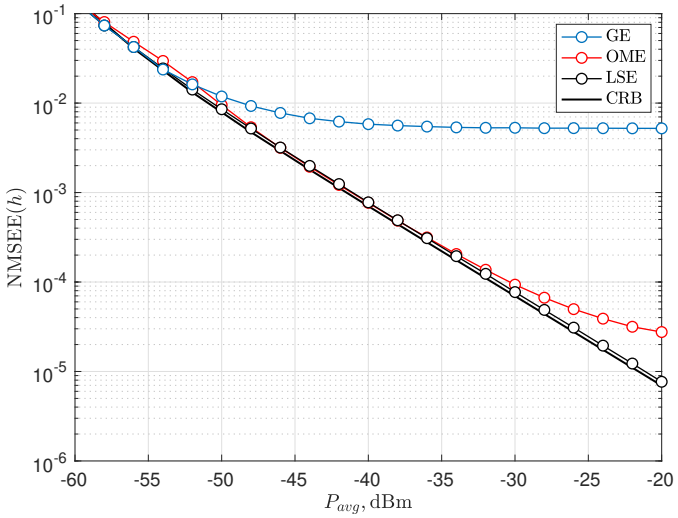

Fig. 4. Normalized MSE for channel gain estimation as a function of P_{avg}, with ε uniformly distributed in $[0, 1)$. Comparisons between LSE, GE and OME.

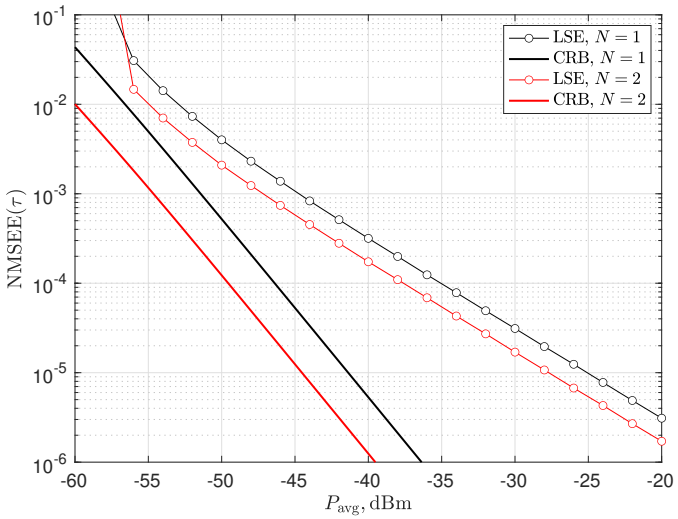

Fig. 5. Normalized MSE for the estimation of τ as a function of P_{avg}, with $\varepsilon = 0$ and $N = 1$ or 2.

a case the data payload is lost anyway due to the incorrect frame acquisition. As is seen, the accuracy of LSE is close to the CRB at any value of P_{avg} (conditioned on $\hat{k}_0 = k_0$), which is quite surprising since the bound has been evaluated by considering the presence of shot noise in the signal model, while the noise statistics are totally overlooked by LSE. This fact suggests that no useful information about the channel coefficient can be extracted from the shot noise statistics. The OME performs similarly to LSE, except for an irreducible floor that appears in the NMSEE curve at large values of P_{avg}. Such a floor is more evident with GE as a consequence of the parabolic interpolation employed by this scheme, which results into some estimation error even in the absence of noise. Extensive computer simulations (not shown for space limitations) reveal that the accuracy of LSE in terms of NMSEE(h) is virtually independent of N. This fact can easily be explained for $\varepsilon = 0$ and in the absence of shot noise, since in these hypotheses the output from an IDF that operates at symbol rate is a sufficient statistic for the ML estimation of h. Our measurements suggest that a similar conclusion also applies in a more general setting, where $\varepsilon \neq 0$ and the received samples are plagued by shot noise.

We now present a last set of experiments illustrating the accuracy of the timing estimates provided by LSE. As a performance indicator, we use the mean square estimation error normalized

to the symbol period T, which is defined as

$$\text{NMSEE}(\tau) = \text{E}\left\{\left(\frac{\hat{\tau}-\tau}{T}\right)^2\right\} \tag{66}$$

with $\hat{\tau}$ given in (64). Fig. 5 shows NMSEE(τ) as a function of P_{avg} for $\varepsilon = 0$ and $N = 1$ or 2. These results are still obtained under the assumption of ideal UW detection ($\hat{k}_0 = k_0$), with the CRB curves taken from (56). In contrast to what was observed for the channel estimates, parameter N has a significant impact on the timing estimation accuracy. Indeed, a gain of approximately 3 dB arises when passing from $N = 1$ to $N = 2$ for both the experimental curves and the relevant bounds. When compared to the CRB, LSE exhibits a remarkable loss of performance, which increases with P_{avg}. To see how this comes about, consider the special case $\varepsilon = 0$, with a bit transition $1 \to 0$ or $0 \to 1$ occurring at $t = kT_c$. In such a situation, two consecutive IDF outputs $x(kT_c)$ and $x(kT_c + T_c)$ placed across the transition are not only characterized by a different mean value, but also exhibit different power noise levels. Such an abrupt variation of the noise power provides useful information for the timing recovery process which is accounted for in the CRB, while it is not exploited by LSE, which operates without taking the noise statistics into account. In our simulation set-up, the amount of shot noise introduced by the APD increases with the average received optical power as specified in (62). This justifies why, for $\varepsilon = 0$, LSE performs poorly with respect to the bound as P_{avg} grows large.

In Fig. 6 we report NMSEE(τ) versus the fractional timing error for $N = 1$ and three different values of P_{avg}. It is worth observing how the performance of LSE is virtually independent of ε, while the relevant CRB steadily increases with ε and comes close to the corresponding LSE curve when $\varepsilon = 0.5$. We can justify such a strong dependence of the CRB on ε by recalling that, in general, two IDF outputs placed around a bit transition exhibit a difference in their average noise power that may prove useful for the purpose of timing recovery. Such a difference achieves a maximum value of $(N_1 - N_0)/(2N)$ when $\varepsilon = 0$ and progressively reduces as ε approaches 0.5. This fact is easily seen if we consider the extreme situation in which $N = 1$, $\varepsilon = 0.5$ and the UW is composed of alternating zeroes and ones. In this scenario, each entry of the noise vector $\mathbf{n}(k_0)$ has the same average power $\sigma_n^2 = (N_0 + N_1)/(2N)$, so that any possible information provided by the shot noise regarding the bit transition is totally lost. This means that in the proximity of $\varepsilon = 0.5$ there is little to gain from exploiting the statistics of $\mathbf{n}(k_0)$ and, consequently, LSE performs close to the CRB.

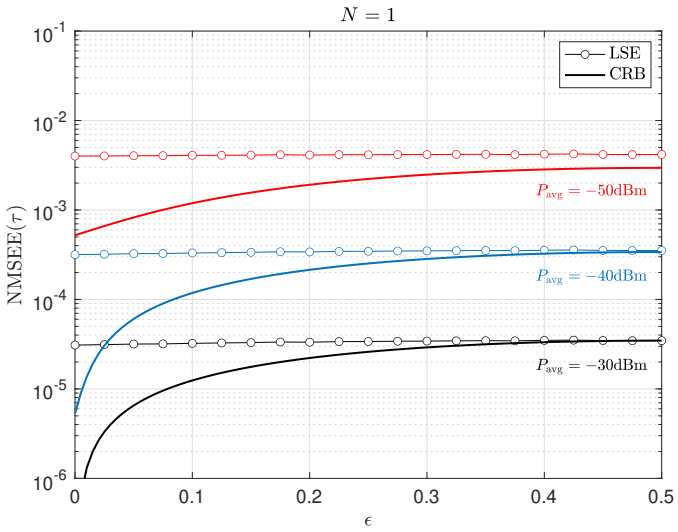

Fig. 6. Normalized MSE for the estimation of τ as a function of ε, for three different values of P_{avg} and $N = 1$.

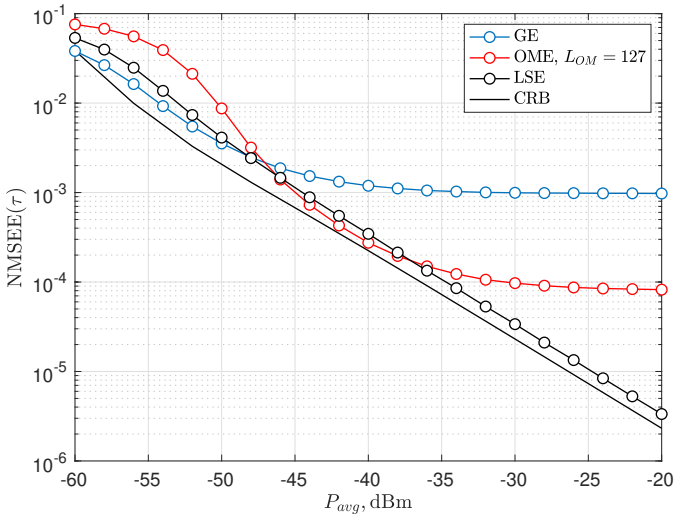

Fig. 7. Normalized MSE for the estimation of τ as a function of P_{avg} with ε uniformly distributed in $[0, 1)$. Comparisons between LSE, GE and OME.

In Fig. 7, LSE is compared with GE and OME in terms of NMSEE(τ) vs. P_{avg}. The oversampling factor is $N = 2$ for GE and $N = 4$ for OME, while LSE operates at symbol rate ($N = 1$). Since the fractional frequency offset ε is uniformly distributed over $[0, 1)$, the CRB is obtained by averaging the expression (56) with respect to ε. At sufficiently large SNR values, we see that the accuracy of LSE is less than 2 dB far from the bound. This seems in contrast to what was observed in Fig. 5, where the LSE and the CRB lines are characterized by different slopes. Such an apparent disagreement can be explained by recalling that the results of Fig. 5 are obtained with $\varepsilon = 0$, which corresponds to a situation where the loss of LSE with respect to the bound is maximum. Hence, when ε varies in the interval $[0, 1)$, we logically expect a certain reduction of this loss, thereby justifying the results of Fig. 7. It is worth noting that both the OME and GE curves exhibit an irreducible floor at large values of P_{avg}. In the medium SNR regime, OME and LSE perform similarly, while GE is marginally better for $P_{\text{avg}} < -50$ dB. In the latter case, however, the accuracy of all investigated schemes is unsatisfactory and the only possible option to achieve acceptable performance is an increase of the UW length.

C. Complexity comparison

We complete our study by comparing the investigated schemes in terms of their computational complexity. In our simulation set-up we have $L_0 = L_T = 63$, while the overampling factor is $N = 1$ for LSE, $N = 2$ for GE and $N = 4$ for OME. Combining these figures with the results shown in Tab. I, it turns out that LSE requires 137 flops per symbol period, while GE and OME needs 250 and 78 flops, respectively. Although OME is less demanding than the other schemes in terms of number of required flops, it operates with an oversampling factor $N = 4$, which represents a strong disadvantage in high-rate FSO communications. A similar drawback emerges with GE, whose application requires the highest number of flops in conjunction with $N = 2$. In contrast, LSE can provide fast synchronization with reasonable complexity and without requiring any signal oversampling.

VI. CONCLUSIONS

We have addressed the problem of channel estimation, timing recovery and frame acquisition in a packet-based FSO communication system employing an OOK modulation format. Since an APD is employed at the receiver as a photodetector, the noise variance is signal-dependent due to the presence of shot noise. By applying the LS estimation principle, we have derived

a scheme, named LSE, which can provide estimates of all the unknown parameters in a joint fashion, so as to speed-up the synchronization process as much as possible. A significant part of this work has been devoted to the evaluation of the CRB for the joint estimation of the unknown parameters, including the signal dependent noise variances. Observing that LSE operates by ignoring the noise statistics, the CRB has proved to be useful for assessing the loss incurred by LSE with respect to an optimum ML synchronization scheme that can effectively exploit the abrupt variations of the noise power as a consequence of a bit transition.

Computer simulations conducted in the presence of thermal and shot noise indicate that the proposed method performs well and, in many situations, its accuracy is close to the relevant CRB. Compared to alternative timing recovery schemes that need signal oversampling, a major advantage of LSE is the possibility of operating with symbol-spaced samples, while requiring an affordable complexity in terms of number of flops. This makes LSE particularly attactive for FSO transmissions, where the symbol rate is extremely high and the cost for signal oversampling may be relevant in terms of hardware equipment.

VII. Appendix A

In this Appendix we highlight the major steps leading to the FIM for the estimation of the unknown parameters $\boldsymbol{\varphi} = \{\varepsilon, h, N_0, N_1\}$. This matrix has entries

$$[\mathbf{F}_{\boldsymbol{\varphi}}]_{k_1,k_2} = -\mathrm{E}\left\{\frac{\partial^2 \Lambda(\boldsymbol{\varphi})}{\partial\varphi(k_1)\partial\varphi(k_2)}\right\} \quad 1 \le k_1, k_2 \le 4 \tag{67}$$

where $\Lambda(\boldsymbol{\varphi})$ is the LLF in (38), while $\varphi(k)$ denotes the kth element of $\boldsymbol{\varphi}$. Bearing in mind (17) and (37), we get

$$\frac{\partial d_k(\varepsilon)}{\partial\varepsilon} = b_k \tag{68}$$

$$\frac{\partial\sigma_n^2(k,\varepsilon,N_0,N_1)}{\partial\varepsilon} = \frac{(N_1-N_0)b_k}{2N} \tag{69}$$

$$\frac{\partial\sigma_n^2(k,\varepsilon,N_0,N_1)}{\partial N_0} = \frac{1-d_k(\varepsilon)}{2N} \tag{70}$$

$$\frac{\partial\sigma_n^2(k,\varepsilon,N_0,N_1)}{\partial N_1} = \frac{d_k(\varepsilon)}{2N}. \tag{71}$$

Then, substituting (38) into (67) and using (68)-(71), after lengthy computations the entries of the FIM are found to be

$$[\mathbf{F}_{\boldsymbol{\varphi}}]_{1,1} = \frac{(N_1 - N_0)^2}{8N^2} \sum_{k=0}^{NL-1} \frac{b_k^2}{\sigma_n^4(k, \varepsilon, N_0, N_1)} + \frac{h^2}{N^2} \sum_{k=0}^{NL-1} \frac{b_k^2}{\sigma_n^2(k, \varepsilon, N_0, N_1)} \tag{72}$$

$$[\mathbf{F}_{\boldsymbol{\varphi}}]_{2,2} = \frac{1}{N^2} \sum_{k=0}^{NL-1} \frac{d_k^2(\varepsilon)}{\sigma_n^2(k, \varepsilon, N_0, N_1)} \tag{73}$$

$$[\mathbf{F}_{\boldsymbol{\varphi}}]_{3,3} = \frac{1}{8N^2} \sum_{k=0}^{NL-1} \frac{[1 - d_k(\varepsilon)]^2}{\sigma_n^4(k, \varepsilon, N_0, N_1)} \tag{74}$$

$$[\mathbf{F}_{\boldsymbol{\varphi}}]_{4,4} = \frac{1}{8N^2} \sum_{k=0}^{NL-1} \frac{d_k^2(\varepsilon)}{\sigma_n^4(k, \varepsilon, N_0, N_1)} \tag{75}$$

$$[\mathbf{F}_{\boldsymbol{\varphi}}]_{1,2} = \frac{h}{N^2} \sum_{k=0}^{NL-1} \frac{d_k(\varepsilon) b_k}{\sigma_n^2(k, \varepsilon, N_0, N_1)} \tag{76}$$

$$[\mathbf{F}_{\boldsymbol{\varphi}}]_{1,3} = \frac{(N_1 - N_0)}{8N^2} \sum_{k=0}^{NL-1} \frac{[1 - d_k(\varepsilon)] b_k}{\sigma_n^4(k, \varepsilon, N_0, N_1)} \tag{77}$$

$$[\mathbf{F}_{\boldsymbol{\varphi}}]_{1,4} = \frac{(N_1 - N_0)}{8N^2} \sum_{k=0}^{NL-1} \frac{d_k(\varepsilon) b_k}{\sigma_n^4(k, \varepsilon, N_0, N_1)} \tag{78}$$

$$[\mathbf{F}_{\boldsymbol{\varphi}}]_{2,3} = [\mathbf{F}_{\boldsymbol{\varphi}}]_{2,4} = 0 \tag{79}$$

$$[\mathbf{F}_{\boldsymbol{\varphi}}]_{3,4} = \frac{1}{8N^2} \sum_{k=0}^{NL-1} \frac{d_k(\varepsilon)[1 - d_k(\varepsilon)]}{\sigma_n^4(k, \varepsilon, N_0, N_1)}. \tag{80}$$

ACKNOWLEDGMENTS

This activity has been supported by the European Space Agency (ESA). Opinions, interpretations, recommendations, and conclusions presented in this paper are those of the authors and are not necessarily endorsed by ESA.

REFERENCES

[1] S. Arnon, J. Barry, G. Karagiannidis, R. Schober, and M. Uysal, *Advanced Optical Wireless Communication Systems*, Cambridge University Press, Jun. 2012.

[2] S. Hranilovic, *Wireless Optical Communication Systems*, Springer Science & Business Media, 2005.

[3] M. A. Khalighi and M. Uysal, "Survey on free space optical communication: A communication theory perspective," *IEEE Communications Surveys & Tutorials*, vol. 16, no. 4, pp. 2231–2258, Fourth quarter 2014.

[4] D. Giggenbach, A. Shrestha, C. Fuchs, C. Schmidt, and F. Moll, "System aspects of optical LEO-to-ground links," in *Proc. of International Conference on Space Optics (ICSO 2016)*, Biarritz, France, vol. 10562, International Society for Optics and Photonics, 2017, p. 105625N.

[5] D. Giggenbach, F. Moll, C. Schmidt, C. Fuchs, and A. Shrestha, "Optical on-off keying data links for low earth orbit downlink applications," *Satellite Communications in the 5G Era*, vol. 79, pp. 307–339, 2018.

[6] L. C. Andrews, R. L. Phillips, and C. Y. Young, "Scintillation model for a satellite communication link at large zenith angles," *Optical Engineering*, vol. 39, no. 12, pp. 3272–3280, Dec. 2000.

[7] M. Toyoshima and K. Araki, "Effects of time averaging on optical scintillation in a ground-to-satellite atmospheric propagation," *Applied Optics*, vol. 39, no. 12, pp. 1911–1919, 2000.

[8] W. C. Lindsey and M. K. Simon, *Telecommunication Systems Engineering*, Englewood Cliffs, NJ: Prentice Hall, 1972.

[9] F. M. Gardner, "A BPSK/QPSK timing-error detector for sampled receivers", *IEEE Trans. on Commun*., vol. 34, pp. 423-429, May 1986.

[10] K. H. Mueller and M. Müller, "Timing recovery in digital synchronous data receivers", *IEEE Trans. on Commun*., vol. 24, pp. 516-531, May 1976.

[11] J.M.H. Elmirghani, "Timing synchronization and jitter-induced performance penalty in optical wireless systems", *IEE Colloquium on Optical Free Space Communication Links*, London, UK, 1996.

[12] V. K. Jain, A. B. Asgill, and P. Bobrek, "Synchronization technique for optical OOK receivers", *IEEE Global Telecommun. Conference (GLOBECOM '91)*, pp. 385-391, Phoenix, AZ, USA, 2-5 Dec. 1991.

[13] K. Kiasaleh, "Delay-and-multiply clock regeneration in APD-based direct-detection optical OOK communication systems", *IEEE Trans. on Commun*., vol. 40, no. 9, pp. 1448-1462, Sept. 1992.

[14] N. Stojanović, C. Xie, F. Karinou, Z. Qiang, and C. Prodaniuc, "Clock extraction for 28 Gb/s OOK receivers in band-limited dispersive optical channels", *2016 Optical Fiber Communications Conf. and Exhibition (OFC)*, Anaheim, CA, USA, 20-24 Mar. 2016.

[15] Y. Gu, S. Cui, C. Ke, K. Zhou, and D. Liu, "All-digital timing recovery for free space optical communication signals with a large dynamic range and low OSNR", *IEEE Photonics Journal*, vol. 11, no. 6, Dec. 2019.

[16] M. Maalej and H. Besbes, "Accurate blind synchronization for free space optical communication systems using 2-PPM modulation", in *Proc. of 15th Int. Wireless Commun. & Mobile Computing Conf. (IWCMC)*, pp. 243-248, Tangier, Morocco, 24-28 June 2019.

[17] Z. Li, A. Tan, Y. Song, Y. Li, J. Chen, and M. Wang, "OOK-assisted adaptive equalization and timing recovery for PAM4 demodulation", in *IEEE Photonics Journal*, vol. 10, no. 2, pp. 1-7, Apr. 2018.

[18] N. Kong and C. N. Georghiades, "Joint synchronization and detection from samples taken through integrate-and-dump", in *Proc. of 25th Asilomar Conference on Signals, Systems & Computers*, pp.1185-1189, Pacific Grove, CA, 4-6 Nov. 1991.

[19] C. N. Georghiades and D. L. Snyder, "Locating data frames in direct-detection optical communication systems", *IEEE Trans. on Commun*., vol. 32, no. 2, pp. 118-123, Feb. 1984.

[20] J. L. Massey, "Optimum frame synchronization", *IEEE Trans. on Commun.,* vol. 20, no. 2, pp. 115-119, Apr. 1972.

[21] G. L. Lui and H. H. Tan, “Frame synchronization for direct-detection optical communication systems”, *IEEE Trans. on Commun*., vol. 34, no. 3, pp. 227-237, Mar. 1986.

[22] A. R. Hammons and F. Davidson, “Near-optimal frame synchronization for free-space optical packet communications”, in *Proc. of Military Commun. Conf. (MILCOM) 2010*, pp. 797-801, San Jose, CA, USA, 31 Oct.-3 Nov. 2010.

[23] M. Morelli, M. Moretti, A. A. D’Amico, and G. Colavolpe, “Frame synchronization for FSO links with unknown signal amplitude and noise power,” *IEEE Wireless Commun. Letters*, vol. 10, no. 7, pp. 1498-1502, Jul. 2021.

[24] K. O. Akande and W. Popoola, “Synchronization of carrierless amplitude and phase modulation in visible light communication”, *Int. Conf. on Commun. (ICC) - 3rd Workshop on Optical Wireless Communications (OWC)*, Paris, France, 21-25 May 2017.

[25] W. Gappmair, “On parameter estimation for bandlimited optical intensity channels”, *MDPI Computation: Special Issue on Optical Wireless Communication Systems*, vol. 7, no. 1, pp. 1-13, Feb. 2019.

[26] X. Zhou and X. Chen, “Parallel implementation of all-digital timing recovery for high-speed and real-time optical coherent receivers,” *Optics Express*, vol. 19, no. 10, pp. 9282-9295, 2011.

[27] M. Oerder and H. Meyr, “Digital filter and square timing recovery,” *IEEE Trans. on Commun*., vol. 36, no. 5, pp. 605-612, May 1988.